

1      **Design of an Anthropomorphic Respiratory Phantom for**  
2      **PET Imaging**

3      David G. Black<sup>1,\*</sup>, Yas Oloumi Yazdi<sup>1</sup>, Jeremy Wong<sup>1</sup>, Roberto  
4      Fedrigo<sup>1,2</sup>, Carlos Uribe<sup>3,4</sup>, Dan J. Kadrmas<sup>5</sup>, Arman Rahmim<sup>1,2,4</sup>,  
5      Ivan S. Klyuzhin<sup>2,4</sup>

6      <sup>1</sup> Department of Physics and Astronomy, University of British Columbia, Vancouver, Canada

7      <sup>2</sup> BC Cancer Research Institute, Vancouver, Canada

8      <sup>3</sup> Department of Functional Imaging, BC Cancer, Vancouver, Canada

9      <sup>4</sup> Department of Radiology, University of British Columbia, Vancouver, Canada

10     <sup>5</sup> Department of Radiology and Imaging Sciences, University of Utah, Salt Lake City, UT,  
11     United States

12     Version typeset December 8, 2020

13     \* Corresponding Author, Email: dgbblack@ece.ubc.ca

15      **Abstract**

16      **Purpose:** Respiratory motion during positron emission tomography (PET) scans can  
17      be a major detriment to image quality in oncological imaging, leading to quantification  
18      errors and false negative findings. The impact of motion on lesion quantification and  
19      detectability can be assessed using anthropomorphic phantoms with realistic anatomy  
20      representation and motion. In this work we design and build such a phantom.

21      **Methods:** We start from a previously-developed anatomically-accurate shell of a hu-  
22      man torso and add elastic lungs with a highly controllable actuation mechanism which  
23      replicates the physics of breathing. To maintain anatomical accuracy in the torso, all  
24      motion mechanisms and actuators are positioned outside of the phantom compartment.

25      **Results:** Tests were carried out to validate the performance of the entire phantom  
26      assembly. The actuation mechanism can produce a plethora of custom respiratory  
27      waveforms with breathing rates up to 25 breaths per minute and tidal volumes up to  
28      1200mL.

29      **Conclusions:** The full mechanical design is described in this paper, as well as a  
30      software application with graphical user interface which was developed to plan and  
31      visualize respiratory patterns. Both are available open source and linked in this paper.  
32      The developed phantom will facilitate future work in evaluating the impact of respira-  
33      tory motion on lesion quantification and detectability.

35      **Keywords:** PET, Quantitative Imaging/Analysis, Motion Management, Phantoms - Phys-  
36      ical, Motion Correction, Anthropomorphic Phantom

# <sup>37</sup> Contents

<sup>38</sup>	<b>I. Introduction</b>	<b>1</b>
<sup>39</sup>	<b>II. Materials and Methods</b>	<b>3</b>
<sup>40</sup>	<b>II.A. Lungs</b> . . . . .	6
<sup>41</sup>	<b>II.B. Breathing Mechanism</b> . . . . .	8
<sup>42</sup>	<b>II.B.1. Piston and cylinder</b> . . . . .	8
<sup>43</sup>	<b>II.B.2. Mounting Plates</b> . . . . .	10
<sup>44</sup>	<b>II.B.3. Linear Actuator</b> . . . . .	11
<sup>45</sup>	<b>II.C. Software and Electrical Design</b> . . . . .	15
<sup>46</sup>	<b>II.C.1. USB Interface</b> . . . . .	15
<sup>47</sup>	<b>II.C.2. Analog Position Control</b> . . . . .	17
<sup>48</sup>	<b>III. Results: Testing and Validation</b>	<b>18</b>
<sup>49</sup>	<b>IV. Discussion</b>	<b>20</b>
<sup>50</sup>	<b>V. Conclusion</b>	<b>21</b>
<sup>51</sup>	<b>VI. Open Source</b>	<b>22</b>
<sup>52</sup>	<b>VII. Acknowledgements</b>	<b>22</b>
<sup>53</sup>	<b>References</b>	<b>22</b>

## 54 I. Introduction

55 Positron emission tomography (PET) imaging is widely used in oncology for tumor detection,  
56 monitoring, and quantification. A leading factor that can adversely affect the quality of  
57 thoracic PET images is respiratory motion during the scans<sup>1</sup>. One of the main negative  
58 effects is the reduction of contrast for small lesions (e.g. cancer metastases)<sup>2</sup>, which worsens  
59 lesion detectability and introduces bias in the measured standardized uptake values (SUVs)  
60 and other metrics<sup>3 4 5</sup>. In normal respiration, the amplitude of diaphragm movement is on the  
61 order of 1.5–2 cm<sup>6</sup>, while deep inspiration may result in 7–13 cm diaphragm displacement<sup>7</sup>.  
62 For clinical PET scanners with spatial resolution around 4–5 mm full-width at half-maximum  
63 (FWHM), motion of this magnitude can lead to effective usable resolution closer to 10 mm<sup>8 9</sup>.  
64 Thus, motion needs to be taken into account in the process of cancer staging<sup>10</sup>. as well as  
65 during image-guided radiotherapy<sup>11</sup>.

66 Since it is impossible to know the ground truth with real subjects, the impact of motion  
67 on PET image quantification is typically assessed using geometrically simple phantoms that  
68 simulate motion of a precisely-known trajectory, such as the QUASAR Phantom (Modus  
69 QA, Ontario, Canada). On the other hand, with continuous advances in PET scanner sen-  
70 sitivity and resolution<sup>12</sup>, as well as development of novel image quantification paradigms<sup>13</sup>,  
71 it becomes of interest to evaluate the effects of respiratory motion under more realistic con-  
72 ditions. Several anthropomorphic phantoms have been developed in the past, each of which  
73 solves a subset of the problems associated with modeling respiratory motion. These phan-  
74 toms are compared in Table 1. While Wilhelm<sup>14</sup> has the most realistic overall motion of any  
75 existing device, it lacks any bone structure, which greatly affects the realism of the phantom  
76 as bone attenuation plays an important role in image quantification. Conversely, Alderson<sup>15</sup>  
77 has bones as well as respiratory and cardiac motion; however its anatomy is simplified. It  
78 also does not support the addition of lesions, which are key in any studies investigating the  
79 effect of motion on image quantification.

80 The goal of this work was to create an anatomically accurate phantom with realistic  
81 modeling of respiratory motion. Our work builds upon an existing phantom previously  
82 developed and tested by Kadrmas et al.<sup>16 17</sup>, henceforth referred to as “Probe-IQ” (Image  
83 Quality Probe). To the best of our knowledge, Probe-IQ to this day has the highest level  
84 of anatomical realism in the field. While highly realistic in PET and, to a lesser extent,  
85 computed tomography (CT) scans, the phantom has previously been completely static and

not used to study motion effects. The motion-enabled phantom described in this paper uses the shell and rib-cage of the original Probe-IQ phantom, but adds custom-built elastic lungs with trachea, and an electronically-controlled actuation mechanism to create realistic respiratory motion.

The Probe-IQ phantom with respiratory motion abilities aims to achieve the following:

#### *Anatomical Accuracy*

- Builds off the static anatomical accuracy of Probe-IQ and achieves realistic lung motion.
- Avoids any unrealistic parts like connecting rods or metal components in the torso.
- All materials carefully selected with reference to mass attenuation coefficients<sup>18</sup> that resemble human tissue.

#### *Breathing Control*

- Able to achieve a wide range of typical breathing rates and tidal volumes (i.e. air displaced between normal inhalation and exhalation). Namely, at least up to 25 breaths per minute at 1L tidal volume. (Typical relaxed breathing is 500mL tidal volume at 15-20 breaths per minute<sup>19</sup>.)
- Has highly controllable, repeatable, consistent breathing motion to generate high quality data, but also can include occasional disrupted breaths or inconsistencies, as would happen in a real patient.

In addition, safety is a concern, as the phantom will be filled with 17.3L of radioactive solution (300 to 1000MBq of radioactivity per scan) for PET acquisitions. The design must avoid leaks, and minimize the chances of spills. Easy fill-ability of the phantom is also desirable to reduce radiation exposure to users and to increase usability.

Table 1: Comparison of existing anthropomorphic phantoms. CM: cardiac motion, RM: respiratory motion, LM: liver motion, SS: skeletal structure.

Name	PET/CT/MRI	CM	RM	LM	SS	Lesions
Probe-IQ + Respiratory motion capabilities	✓ / ✓ / ×	✗	✓	✓	✓	✓
Probe-IQ <sup>16 17</sup>	✓ / ✓ / ×	✗	✗	✗	✓	✓
Wilhelm <sup>14</sup>	✓ / ✓ / ✓	✓	✓	✓	✗	✓
Alderson <sup>15</sup>	✓ / ✓ / ×	✓	✓	✗	✓	✗

109

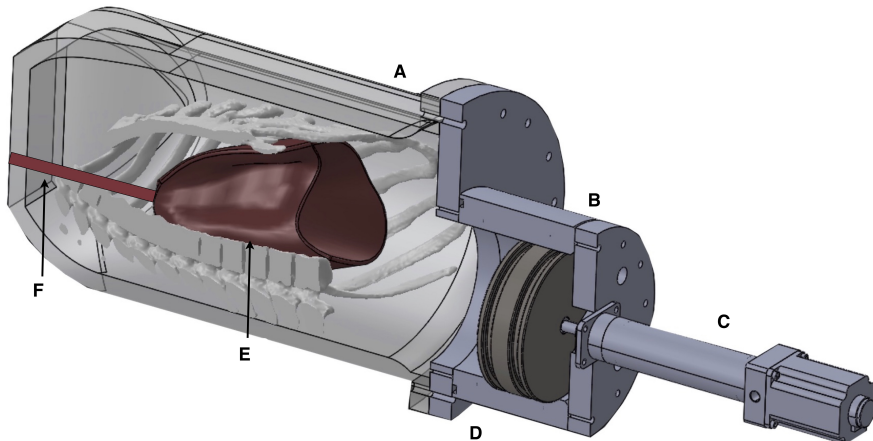


Figure 1: Overview of phantom design. A: existing thorax shell and bone structure (liver and heart included but not pictured). B: Piston and cylinder for torso volume modulation. C: linear actuator. D: custom-designed base-plate allows compatibility with existing Probe-IQ phantom. E: flexible lung inserts of silicone elastomer. F: breathing tubes (trachea) connect lungs to atmosphere to allow breathing.

## <sup>110</sup> II. Materials and Methods

<sup>111</sup> The addition of lung motion to the Probe-IQ phantom involves three main components: 1)  
<sup>112</sup> elastic lungs, 2) an actuation method, and 3) a control system (electronics and software).  
<sup>113</sup> The overall structure can be seen in Fig. 1 and all design files and code can be accessed in  
<sup>114</sup> the Open Source Section at the end of this paper. The lungs are located inside the rib cage of  
<sup>115</sup> the existing Probe-IQ phantom (A), and surrounded by a radioactive water solution creating  
<sup>116</sup> the background observed in PET images. The lungs are connected to the atmosphere by a  
<sup>117</sup> breathing tube (trachea) (F), which can be sealed at the neck. The actuating mechanism is  
<sup>118</sup> positioned below the phantom (B, C, D), where the pelvis of a human would be located. It is  
<sup>119</sup> outside the field of view of the PET scanner so as not to create image artefacts. The phantom  
<sup>120</sup> operates by piston-actuated passive breathing, as explained below and seen in figure 2.

<sup>121</sup> Achieving respiratory motion with the lungs is possible through a variety of mechanisms,  
<sup>122</sup> which fall into two main classes.

<sup>123</sup> First, the lungs can be directly inflated using air pumps or compressors. This is the  
<sup>124</sup> most obvious approach, but involves a number of complicating factors. The lung volume  
<sup>125</sup> cannot simply increase inside a sealed, rigid torso filled with an incompressible fluid. An  
<sup>126</sup> overflow tube or expanding section of the torso would be required. The former would create  
<sup>127</sup> the risk of leakage, while the latter would require a powerful compressor. Furthermore,  
<sup>128</sup> control is much more difficult with a pneumatic system and would require a great increase

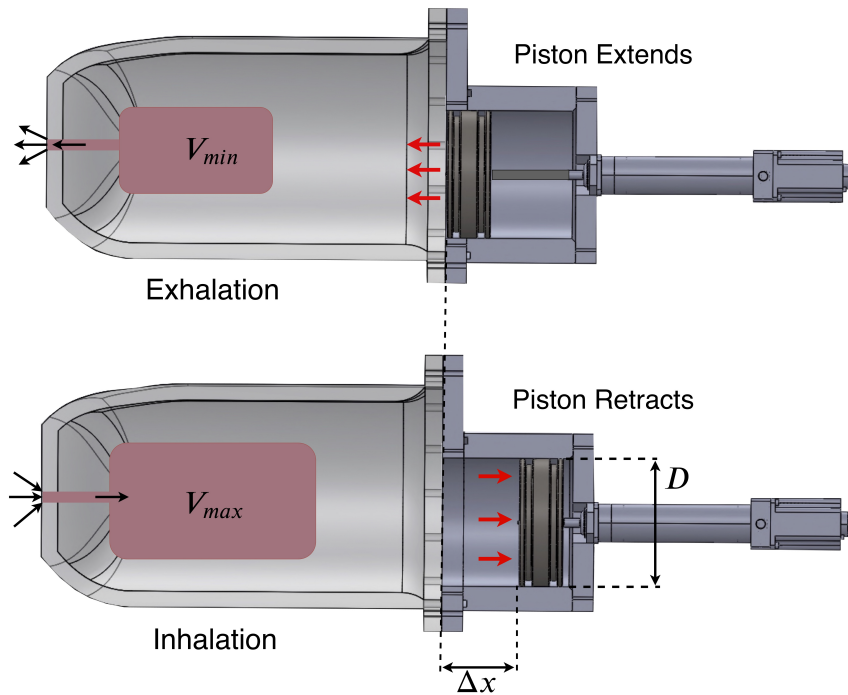


Figure 2: Respiration modeling by modulating the volume of the phantom, mediated by incompressible fluid. Air flows into and out of the lungs through the trachea as the piston extends and retracts.

129 in complexity.

130 The second, and preferred method is to instead modulate the volume or pressure of the  
 131 whole phantom in a manner analogous to actual respiratory breathing. Since the phantom  
 132 is sealed, rigid, and entirely filled with water, except for the air-filled lungs, changing its  
 133 volume by  $\Delta V$  induces an equal volume change of  $\Delta V$  in the lungs. Instead of compressing  
 134 the air in a sealed set of lungs, the pressure requirement of the actuating mechanism can  
 135 be dramatically decreased by opening the lungs to the atmosphere once the phantom has  
 136 been filled and sealed. Contrary to intuition, the lungs will not collapse under the pressure  
 137 of the water since the water volume is constant and cannot expand to fill the vacant space  
 138 created if the lungs were to collapse. In effect, a relative negative pressure is created in  
 139 the liquid above the lungs, just as human breathing relies on negative intrapleural pressure.  
 140 Now, when the volume of the torso is changed, that volume of air is simply exhaled to or  
 141 inhaled from the atmosphere (figure 2).

---

## II. MATERIALS AND METHODS

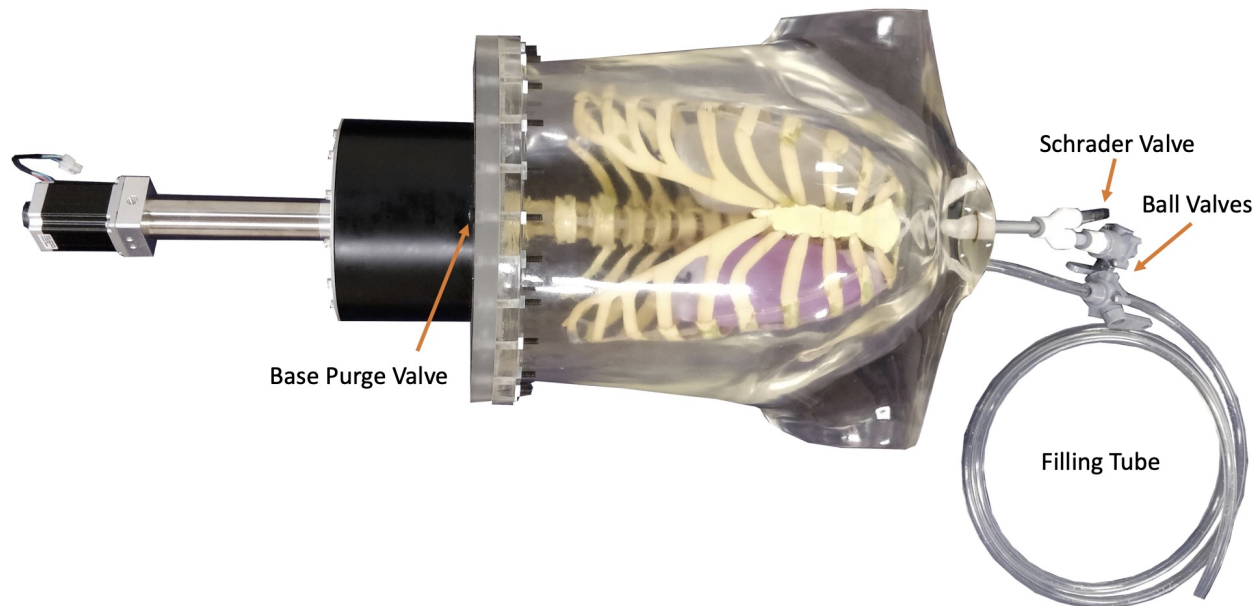


Figure 3: Assembled phantom with filling system

- 142 To prepare the phantom for imaging, the following steps are taken:
- 143 1. The lungs, organs, and bones are positioned inside the thorax.
- 144 2. The lungs are inflated to their maximum capacity via a Schrader valve and a manual
- 145 pump and sealed (figure 3).
- 146 3. The piston is moved to its most retracted position (i.e. the phantom is at maximum
- 147 volume), and the base plate is attached.
- 148 4. The torso is completely filled with radioactive water solution using the ports in the
- 149 neck. A valve in the base plate, at the highest point in the torso, is used to release the
- 150 displaced air (figure 3).
- 151 5. The torso is sealed, and the lungs opened to the atmosphere.

152 Since the torso is rigid and sealed, its volume cannot change, so the lungs remain inflated.

153 At this point, the lung volume can be fine-tuned by opening the water-filling port and/or

154 base purge valve while pumping air into the lungs through the Schrader valve using a manual

155 pump. Thus, any small changes or issues can be rectified. With the phantom set up, the

156 user can define a wide variety of respiratory patterns, rates, and volumes using a graphical

157 user interface. The piston then moves along the defined trajectory for the duration of a scan,

158 causing the lungs to expand and contract due to the changes in pressure. The piston motion

can also be coupled directly to the lungs using thin cables, which are not visible in the PET scan. The next three sections explain the lungs, breathing mechanism, and software in more detail.

## II.A. Lungs

The lung shapes were derived from a CT scan of an adult male lung and simplified using mesh editing software (Blender Foundation, Amsterdam) to reduce the cardiac notch and make the right and left lungs more symmetrical (figure 4). This was done primarily for ease of fabrication, but also to avoid unpredictable expansion and contraction of complex shapes which differ between the lungs. The lungs were designed to have a realistic adult size post-exhalation, with a volume of 1650ml each. This ensures that during normal breathing the lungs only expand, and do not compress or fold in an irregular manner. The dimensions of the lungs are approximately 18.0cm (height) by 10.0cm (width) by 12.7cm (depth) (figure 4). The lungs have uniform wall thickness of 2mm and can optionally be coupled directly to the piston using thin cables to force a specific longitudinal flex pattern.

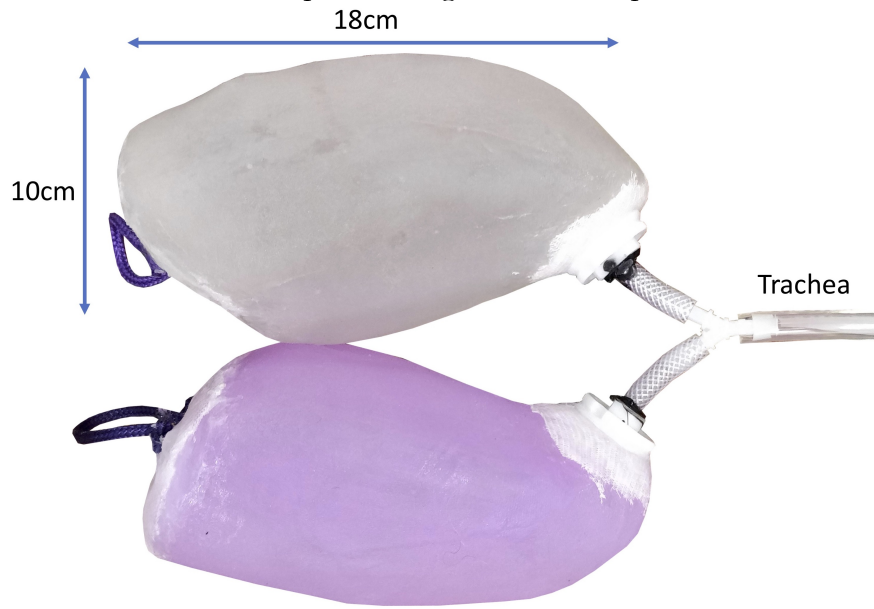


Figure 4: Elastic silicone lungs with bronchi and trachea. Bottom loops can be used to couple the lung motion directly to the piston.

A thru-wall fitting commonly used in prosthetics was custom manufactured using Delrin plastic (figure 5). This is attached medially near the top points of both lungs to connect air tubes which lead through a Y-connector to a single tube to the outside of the phantom, much like bronchi connecting to the trachea. One of three ports in the neck area of the

phantom provides the inlet for the breathing tubes. The lungs are held in place in the superior/inferior axis using the trachea, and in the lateral and anterior/posterior axes using the rib cage. At the inlet of the trachea, near the neck of the phantom, another Y-connector splits the airway into a large ball valve and a Schrader valve which are used to alternatively pressurize and seal the lungs or allow free airflow (figure 3).



Figure 5: Original (left) and custom manufactured plastic (right) thru-wall fitting (ESP LLC, New Jersey, USA) used to attach trachea to the lungs. The lung silicone is compressed between the twin flanges and creates an air-tight seal.

The lungs were manufactured from Chlorosil-35 (Ottobock, Germany), a two-part, silicone-based elastomer with Shore A hardness 35. Following high temperature vulcanization, this material is durable, long-lasting, and thermostable, yet flexible to allow contraction and expansion. The material was previously tested in another phantom<sup>14</sup>. The lung manufacturing process was as follows:

1. A negative mold was 3D-printed out of polylactic acid (PLA) in two halves due to size constraints in 3D-printing.
2. Dental plaster was poured into the negative mold using a hole at the base.
3. Once the plaster dried, it was extracted from the mold and put in a polyvinyl alcohol (PVA) bag. This bag prevents the Chlorosil catalyst from reacting with the plaster.
4. The Chlorosil was rolled onto the positive dental plaster mold of the lungs and placed in an evacuated plastic bag to obtain a uniform shape and thickness.
5. The mold with the rolled Chlorosil was placed in an oven at 200°C for 12 hours to cure the Chlorosil.
6. A thin piece of stiffer plastic with a mounting point for a cable was placed in a silicone

197 pocket at the base of each lung.

- 198 7. The mold was removed from inside the Chlorosil-35 lungs through the breathing hole  
199 to which the trachea will be attached; this is possible because the material is highly  
200 flexible.

201 **II.B. Breathing Mechanism**

202 To modulate the volume, both a rubber “diaphragm” membrane stretched across the entire  
203 phantom base and a piston mechanism were considered. After preliminary testing, the  
204 diaphragm mechanism was found to be unreliable, so the piston mechanism was chosen.  
205 This consists of a large cylinder attached directly to the base plate of the phantom. A piston  
206 is driven back and forth in the cylinder using a linear actuator to create the volume change.  
207 The actuator works against the piston friction, water viscosity/inertia, and elastic forces in  
208 the lungs.

209 The mechanism consists of three major components: the piston and cylinder (figure 6),  
210 the base and mounting plates, and the linear actuator. Each is described below, before  
211 outlining their cumulative capabilities. The assembled mechanism is shown in figure 8.



Figure 6: Left: Piston with dual O-rings; Center: Cylinder with O-ring to seal against base plate; Right: Piston in Cylinder. Threaded blind hole in piston to couple lung motion is visible.

212 **II.B.1. Piston and cylinder**

213 A key consideration in the piston and cylinder design was dimensional tolerance and stability.  
214 To ensure a good seal, specific dimensions with low tolerances had to be chosen, according  
215 to the Parker O-ring Handbook for dynamic sealing. To achieve and maintain the tight  
216 tolerances (eg.  $\pm 0.1\text{mm}$  over a 14cm diameter) while avoiding attenuation and scatter from  
217 metallic components, both the piston and cylinder were manufactured from Delrin acetal  
218 plastic. Delrin is known to be dimensionally stable and machinable. It has a low water

absorption of 0.25% (according to McMaster-Carr), which allows it to keep its shape when in contact with water. Furthermore, Delrin has a low friction coefficient of 0.2, which reduces piston-cylinder friction and greatly decreases the required actuator load<sup>20</sup>. Beyond material choice, the cylinder was designed with thick, 27-mm walls to avoid any warping. A 3.8-mm long chamfer at the mouth of the cylinder ensures easy insertion of the piston without scratching any of the surfaces important for the seal.

Two opposing factors played a role in determining the inner diameter of the cylinder. The larger the diameter, the smaller the piston displacement has to be for a given volume change, and thus the lower the speed requirement on the linear actuator. However, a larger piston is harder to machine within tolerance and to fit onto the base plate. A diameter of 14cm was chosen as a compromise. At this diameter, the piston displacement for a given volume change is approximately equal to the axial lung extension for a given tidal volume<sup>7</sup>. For example, a piston movement of 3cm leads to a volume change of 500ml, which is a typical relaxed adult tidal volume. According to Wade et al.<sup>7</sup>, the lungs should very roughly extend on average 1.5cm for 500ml tidal volume, though this varies widely between individuals. Ultimately, with the chosen dimensions, the change in the torso's (and thus also lungs') volume,  $\Delta V$ , is given by:

$$\Delta V = \frac{\pi}{4} D^2 \Delta x = \frac{\pi}{4} (14\text{cm})^2 (\Delta x) \quad (1)$$

where  $D$  and  $\Delta x$  are given in Fig. 2. The system's stroke is 8cm, so tidal volumes of up to 1232ml are possible, which constitute realistic deep breaths.

The piston has 2 O-ring grooves which ensure alignment inside the cylinder and provide a watertight dynamic seal (Fig. 7). The actuator-side groove is 6% (0.4mm) deeper, allowing for smaller %-compression in the backup O-ring. This reduces the friction slightly but maintains sufficient level of seal to be used as backup. A vent hole connects the inter-O-ring space with the atmosphere in order to avoid pressure traps which can occur in double O-ring configurations. The chosen O-rings are size -429, which have the largest cross-section for the diameter, and thus provide a large contact patch and effective sealing. To compromise between breakaway friction and running friction, 70A durometer Buna-N rubber O-rings were chosen. Buna-N rubber is stronger and more resilient and puncture resistant than other rubbers, making it a good choice for this wear-intensive application. In addition, it does not break down easily under influence of radiation. X- and circular-profile rings were

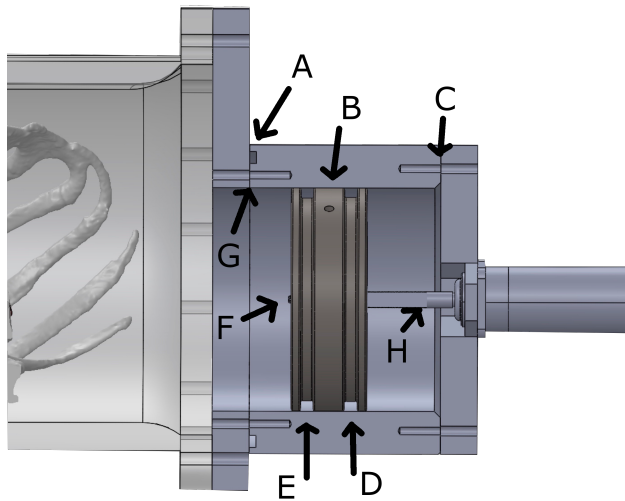


Figure 7: Cross-section of the piston drive mechanism. A: Cylinder face O-ring groove. B: Inter-O-ring vent hole. C: Actuator mounting plate screw holes. D: Backup O-ring groove. E: Main O-ring groove. F: Insert for mounting piston-lung motion-coupling cable. G: Cylinder to base plate mounting screw holes. H: Linear actuator threaded, male rod end mates directly with piston.

250 tested, but no major difference in performance was detected.

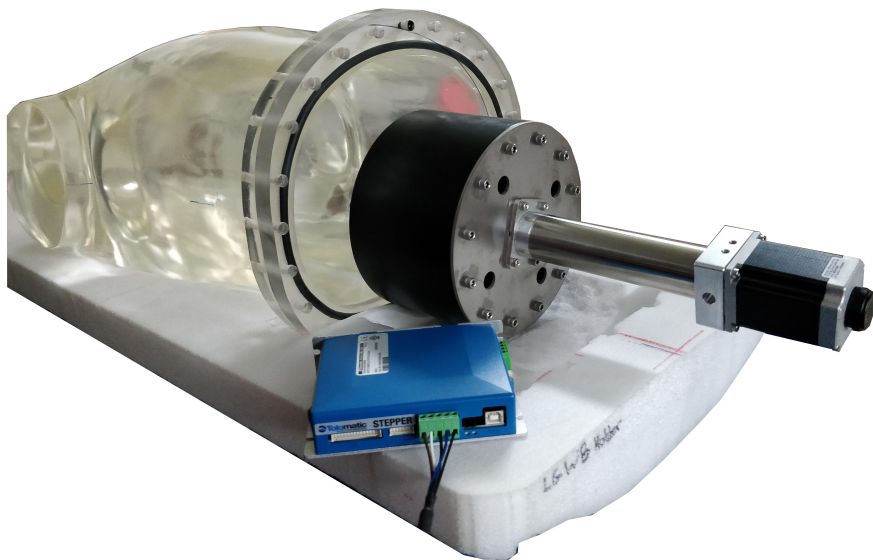
251 The cylinder's inner surface was honed to  $8\text{-}16 \mu\text{in}$  RA roughness. An O-ring groove was  
 252 milled into one end of the cylinder (part A in Fig. 7), with the mounting screws located  
 253 radially inside the groove to avoid leaks through the screw holes. Twelve  $1/4\text{-}20 \times 1"$  steel  
 254 socket-cap screws fasten the cylinder to the base plate. The actuator mounting plate is  
 255 attached in the same manner, but with no O-ring, and the flanged actuator is mounted  
 256 directly to this plate. In this way, misalignment is minimized, and the whole structure is  
 257 modular and easy to assemble and disassemble, for example to add or remove O-rings. The  
 258 linear actuator has an  $M12 \times 1.75$  threaded male rod end, which screws directly into the  
 259 piston, leaving minimal clearance between piston and mounting plate in order to maximize  
 260 the positional range of the piston. An identical threaded hole was made on the opposite  
 261 side of the piston, into which an insert can be screwed to attach a cable to the lungs.  
 262 Alternatively, a rod can be attached here to move an internal diaphragm, or the hole can be  
 263 left empty. This gives flexibility in mounting and motion options.

## 264 II.B.2. Mounting Plates

265 Two plates were made to mount the respiration mechanism to the existing Probe-IQ phantom,  
 266 and to attach the linear actuator to the cylinder assembly. To ensure compatibility

267 with Probe-IQ, a CT scan was taken of the phantom, and the base dimensions extracted as a  
268 SolidWorks file. The plate was fabricated from 1" thick polycarbonate to avoid backscatter  
269 that could be caused by metal. While the overall shape could be made using a waterjet  
270 cutter, a mill had to be used for all the screw holes since the waterjet piercing thick, rela-  
271 tively brittle polycarbonate causes local shattering. A large, central hole was included for  
272 the piston, as well as 36 1/4-20 holes for mounting the cylinder to the base plate and plate to  
273 the phantom base flange in a secure, sealed manner with the load distributed evenly. Finally,  
274 an 8-32 hole was drilled and tapped into the plate at the highest point of the torso cavity to  
275 purge air. The hole is sealed using a flat-head screw with a rubber gasket washer.

276 As the second plate is further away from the scanner's gantry, and supported fully by  
277 the cylinder, it was fabricated from 3mm-thick aluminum for weight, strength, and ease  
278 of fabrication. The plate was entirely waterjet cut, and included mounting points for the  
279 cylinder and actuator. The actuator has a front flange which is mounted directly to the  
280 plate to minimize the risk of misalignment. Furthermore, 4 additional holes were included  
281 to provide venting for the piston and avoid pressure build-up. Though no O-ring is present,  
282 this plate effectively seals in any small leaks that potentially make it through the piston  
O-rings.



283 Figure 8: Assembled breathing mechanism with empty phantom.

284 **II.B.3. Linear Actuator**

285 The actuator type and model were selected based on the criteria outlined in Table 2, as well  
286 as cost.

Table 2: Linear actuator design requirements

Criterion	Desired	Chosen Actuator
Speed	54mm/s	167mm/s
Stroke	90mm	90mm
Force	900N	890N
Duty Cycle	100%	100%
Durability	High	5200-scan estimated life
Controllability	High	See in text
Weight	Low	$\approx 1.5\text{kg}$

We set out to achieve a 1000ml tidal volume at 25 breaths per minute. While the piston was designed to provide up to 1232ml tidal volume, and the 90mm actuator stroke supports the full range of piston motion, the actuator must be fast enough to reach 25 breaths per minute at this amplitude.

By using Equation 1 and noticing that a single breath involves both extension and retraction of the actuator, we find an expression for speed,  $\dot{x}$ , in mm/s as a function of breathing rate,  $\nu$ , and amplitude,  $V$ , in breaths per minute and ml:

$$\dot{x} = \frac{2\nu V}{\frac{\pi}{4}14^2 \cdot 60} \approx \frac{\nu V}{461.8} \text{mm/s} \quad (2)$$

Hence, to fulfil the design objective, a linear speed of at least 54mm/s is required (assuming the actuator accelerates instantly, which is a reasonable assumption: the chosen actuator has a max acceleration of 1667mm/s<sup>2</sup>).

With some simplification, the required force is approximately the sum of the piston friction ( $F_f$ ), the water inertia ( $F_i$ ), and the elastic stretching of the lungs ( $F_e$ ):

$$F = F_f + F_i + F_e \quad (3)$$

From the Parker O-Ring Handbook,  $F_f = f_c L_p + f_H A_p$  where (assuming we are using the -429 O-ring):

- $f_c = 0.933$  is the O-ring compression friction
- $L_p = 17.29\text{in}$  is the seal rubbing surface length
- $f_H = 10$  is the fluid pressure friction
- $A_p = 3.97\text{in}^2$  is the projected seal area.

Thus, the approximate piston friction is  $F_f = 250\text{N}$ .

To calculate the inertial force, assume the actuator accelerates to the 54mm/s velocity within 0.5cm. This corresponds to an acceleration of  $a = \frac{(0.054\text{m/s})^2}{2 \cdot 0.005\text{m}} = 0.292\text{m/s}^2$ . While

310 most of the water in the phantom does not move much during the acceleration, at least the  
 311 water that was in the piston will be accelerated, in addition to some water in the rest of  
 312 the phantom. Suppose, then, that the total volume of water being accelerated is twice the  
 313 maximum tidal volume - i.e. 2000ml - which is 2kg. Then

$$314 \quad F_i = (0.292m/s)(2kg) = 0.58N \quad (4)$$

315 This is negligible compared to the frictional force. Even if we took the whole 17.3kg of  
 316 water to be accelerating, it would still only constitute  $5N$ . This can therefore be ignored.  
 317 Similarly, the static pressure on the piston can be ignored because the lungs in the water are  
 318 at atmospheric pressure, and the piston sits at almost the same height as the lungs. Thus,  
 319 the water pressure on the front of the piston and the air pressure on the back effectively  
 320 cancel out.

321 The pressure required to stretch the lungs is more difficult to derive. To simplify the  
 322 problem, let us assume that the lungs are cylindrical, and use the thin-wall approximation  
 323 to find the hoop stress in one lung. This, however, also assumes that Hooke's Law holds for  
 324 rubber-like elastomers. Merrit and Weinhaus<sup>21</sup> found that this is not the case, and that after  
 325 an initial linear section, the required pressure to increase the radius sharply falls off. Thus,  
 326 Hooke's Law provides a rough, very conservative estimate. Let  $\ell, r, t$  be the cylindrical lung's  
 327 length, radius, and wall thickness respectively, and  $\ell_0 = 200\text{mm}$ ,  $r_0 = 52\text{mm}$ , and  $t_0 = 2\text{mm}$   
 328 be the initial values. These give the expected initial volume of 1700ml, as well as an initial  
 329 material volume of  $V_0^{mat} \approx 2\pi r_0 t_0 (\ell_0 + r_0) = 21000\text{mm}^3$ . Using the incompressibility of  
 330 rubber,  $V_0^{mat} = V_f^{mat}$ , so the wall thickness relates to the length and radius by:

$$331 \quad t \approx \frac{21000}{r(\ell + r)} \quad (5)$$

332 Now using hoop stress,  $\frac{r\Delta P}{t} = \sigma_H$ , and Hooke's Law,  $\sigma_H = \epsilon_H E = \frac{t_0 - t}{t_0} E$ , we obtain an  
 333 expression for the required pressure differential applied by the piston:

$$334 \quad \Delta P = \frac{t(t_0 - t)}{rt_0} E \quad (6)$$

335 Combining Equations 5 and 6:

$$336 \quad \Delta P = \frac{21000}{r^2(\ell + r)} \left( 1 - \frac{21000}{rt_0(\ell + r)} \right) E \quad (7)$$

337 This pressure is exerted evenly across the piston surface, so using  $F = PA$  we find  $F_e$ :

$$338 \quad F_e = (0.14)^2 \frac{\pi}{4} \frac{21000}{r^2(\ell + r)} \left( 1 - \frac{21000}{rt_0(\ell + r)} \right) E \quad (8)$$

339 The elastic modulus,  $E$ , of silicone rubbers can be estimated roughly from the Shore A  
340 durometer using Ruess' Equation:  $\log_{10} E = 0.0235S - 0.6403$ <sup>22</sup>. Since the lung silicone  
341 has Shore A hardness 35,  $E \approx 1.5\text{MPa}$ . Thus we can finally calculate the force required to  
342 stretch the lungs. We want a 1000ml volume increase and about 6.6cm lung extension<sup>7</sup>, so  
343 we take  $\ell = 266\text{mm}$  and  $r = 56.8\text{mm}$ . Then  $F_e = 199\text{N}$ .

344 According to Equation 3, then, a conservative estimate for the maximum force required  
345 from the actuator is  $F = 450\text{N}$ . Applying a factor of safety of 2, considering that these  
346 calculations were approximate, piston friction could increase with wear, foam around the  
347 lungs could increase the pressure requirement, and a second O-ring could be added, with  
348 unknown effect, the linear actuator should be able to supply around 900N of force.

349 To move the piston, a lead-screw actuation mechanism is preferred because of its superior  
350 controllability over pneumatic cylinders and other types of linear actuators. The phantom  
351 has to breathe continuously for the duration of the scan, which can be around 30 minutes,  
352 so the duty cycle has to be 100% for extended periods of time. Many actuators use ACME  
353 screws, a specific thread geometry which can only operate at about 15% duty cycle. Instead,  
354 a ball screw mechanism, which has much less friction, allows for continuous use and a long  
355 lifetime.

356 Based on these criteria, an ERD15 (Tolomatic, USA) ball-screw linear actuator was  
357 chosen, along with a Nema-23, 2-stack stepper motor with encoder feedback. This relatively  
358 low-cost actuator is designed to run continuously and fulfills the load, stroke, and speed  
359 requirements. Assuming we carried out 30 minute scans at the calculated force, at 25  
360 breaths per minute and 1000ml tidal volume, the actuator would have an estimated life of  
361 5200 scans (Fig. 9). The ERD's low profile and simplicity allow it to be mounted as seen in  
362 Fig. 8.

363 According to the manufacturer specifications, the actuator position is accurate to within  
364 0.03mm per cm of movement<sup>23</sup>, which translates to a volumetric error of up to 0.3ml per  
365 100ml volume change, using Equation 1. In addition, the 1.8°/step stepper motor combined  
366 with the 5mm-lead ball screw mechanism, as well as 2000-count encoder feedback facilitate  
367 exact velocity and acceleration control.

368 The force analysis was verified during testing by running the actuator at 40% force,  
369 where it stalled, and then at 60%, where it ran smoothly. This implies the required force  
370 is around 50% of the actuator's force capability, which, given the chosen safety factor of 2,

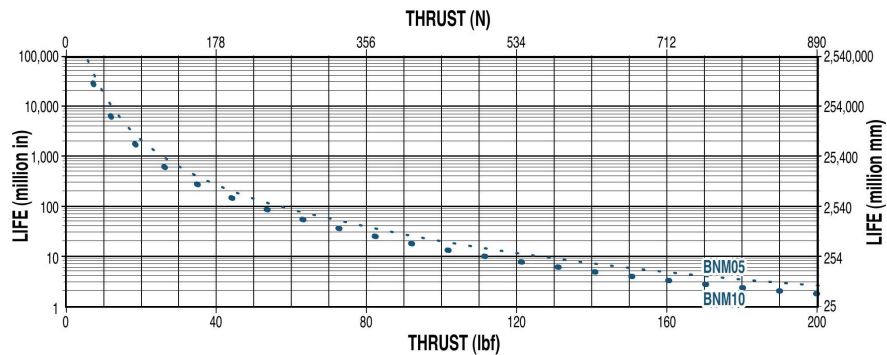


Figure 9: Tolomatic ERD15 BNM05 actuator expected life. At 450N, the life is 508 million mm, which corresponds to about 5200 scans. (Image from Tolomatic.com)

<sup>371</sup> means the required force corresponds closely to the derived value.

## <sup>372</sup> II.C. Software and Electrical Design

The Tolomatic ERD15 actuator is driven by a stepper motor with encoder feedback, which is in turn powered by a 120W, 48V power supply, and controlled by stepper driver hardware from Tolomatic. The goal in this control system is to create realistic, consistent, repeatable lung motion with flexibility in breathing rate and amplitude, as well as the ability to include breathing inconsistencies for added realism. Two distinct control methods were created for the phantom and are described below. The first is simple and fast to set up while the second provides more realism, so each is useful in different applications.

380 First, a free Windows application (described below) can be used to communicate with  
381 the stepper driver over USB to configure the actuator. This option is explored in-depth  
382 below. The second option is analog position control. Here, a 0-10V analog signal can be  
383 input to the driver, which moves to the corresponding position. Control through ethernet  
384 and Modbus RTU over RS-485 are also possible, but neither was investigated in this work.

### 385 II.C.1. USB Interface

The actuator manufacturer provides a software interface called Tolomatic Motion Interface (TMI) to communicate with its stepper controllers over USB. While the software is primarily used to configure the driver by setting acceleration, deceleration, maximum velocity, error states and more, it can also be used to directly control the actuator's movement. In 'Indexing Mode' up to 16 moves can be defined, each with a certain acceleration, deceleration, velocity, and goal position. Any of these moves can then be chosen and combined in any order to form a repeating series of up to 16 moves. Taking the simplest example, one may define just

393 2 moves, one to 45mm, and one to 1mm, and cycle between these two positions indefinitely.  
 394 By combining more positions, however, and altering their accelerations and decelerations, a  
 395 wide variety of breathing patterns can be achieved, including realistic respiratory cycles.

396 The problem with this method is that visualizing what the respiratory cycle will look  
 397 like based on a series of linear position, velocity, and acceleration values is difficult. A  
 398 graphical user interface (GUI) was therefore developed in Python to allow motion planning  
 399 and visualization of the lung volume as a function of time (figure 10).

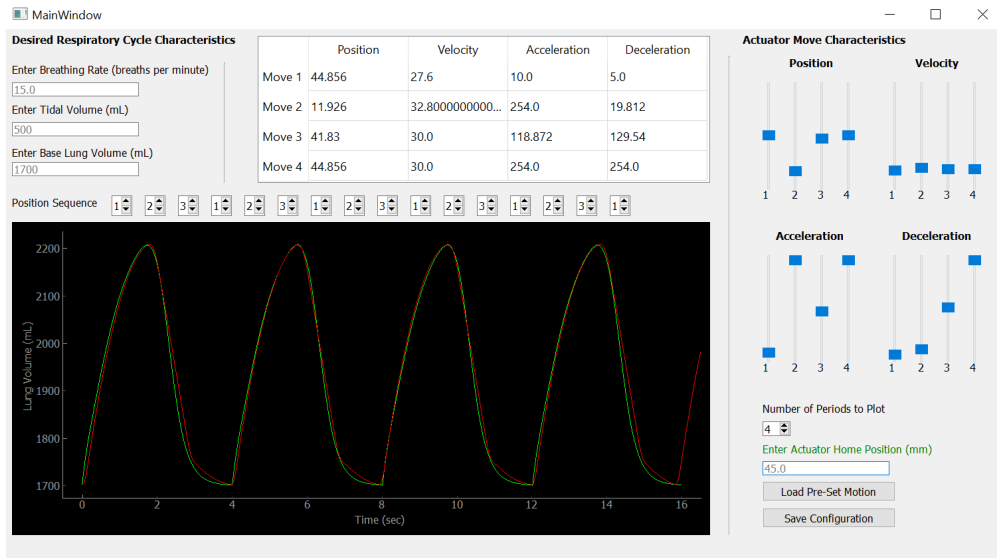


Figure 10: Screenshot of motion planning application. The green curve is the desired respiratory cycle, while the red is the pattern carried out by the phantom based on the GUI inputs.

400 In the application, the user can define the breathing rate, amplitude, and base lung  
 401 volume. We used published models<sup>24</sup> to identify a physiologically representative equation  
 402 for a respiratory curve (Equation 9,  $x$  = amplitude,  $t$  = time), which can be scaled and  
 403 shifted to match the desired, user-defined breathing parameters. This curve is plotted in  
 404 green in figure 10.

$$x = e^{-1.71668t} \frac{0.0106 + 2.3313t + 0.535t^2 + 3.9594t^3}{2.3062 + 0.3517t - 0.6487t^2 + 0.1177t^3} \quad (9)$$

405 The user can then define up to 4 moves with position, velocity, acceleration, and decel-  
 406 eration, and place them in any order. The corresponding motion profile is generated through  
 407 iterative kinematic simulation of the actuator, and plotted in real time, in red in Fig. 10,  
 408 as the parameters are changed. With the red actuator plot overlaid onto the green desired  
 409 plot, the optimal set of motion parameters can be determined. It is also possible to save  
 410

411 configurations in automatically-formatted JSON files to be loaded later.

412 This control method is simple because the respiratory cycle is visualized, input into  
413 user-friendly software, and relayed to the actuator directly over USB. While a variety of  
414 motions can be achieved in this manner, it is nonetheless limited by the discrete nature of a  
415 set of individual moves. To overcome this problem, at the cost of simplicity, analog control  
416 can be used.

417 **II.C.2. Analog Position Control**

418 The second method controls the ERD15 actuator using a 0-10V analog signal. The voltage  
419 range is mapped onto the positional range of the actuator so that a given voltage causes the  
420 actuator to move to that position. The move occurs with predefined acceleration, decelera-  
421 tion, and maximum velocity, which can be configured using the Tolomatic Motion Interface  
422 software, but is non-blocking; i.e. a new position command can be given before the current  
423 position has been reached, and the actuator will immediately move towards the new position.  
424 In this way, arbitrary continuous waveforms can be realized by the actuator, if they do not  
425 exceed the configured acceleration and velocity values.

426 Figure 11 shows the setup used to generate the analog signal. The voltage range is  
427 configurable using the Tolomatic software, and was set to 0-3.3V, which was provided by  
428 an MCP4725 Digital to Analog Converter (DAC), controlled via the I2C GPIO pins of a  
429 Raspberry Pi microcomputer. The encoder feedback is read by the Raspberry Pi, and any  
430 control software is run on the Raspberry Pi.

431 For the actuator to respond to the analog input voltage, analog control must be enabled  
432 through a digital input. The digital I/O operates on 28V logic (18-28V is considered high)  
433 with respect to the digital common pin (COM). Thus, digital COM is tied to the power  
434 supply ground, and a voltage divider is used to provide the 24V needed to enable motion.  
435 An N-channel MOSFET whose gate voltage is set by the Raspberry Pi switches the enable  
436 input between 0 and 24V. The MOSFET gate is pulled down to ground through a  $1\text{M}\Omega$   
437 resistor and attached to the Pi through a  $100\Omega$  resistor to prevent parasitic ringing. The  
438 voltage divider uses  $100\text{k}\Omega$  resistors so the maximum current draw is 0.24mA, which does  
439 not affect the operation of the actuator.

440 With this setup, arbitrary waveforms can be saved as CSV files on the Raspberry Pi. A  
441 Python program converts the volumetric data to actuator positional curves using the piston  
442 geometry, and then to voltages using the voltage-position mapping. The voltages are sent

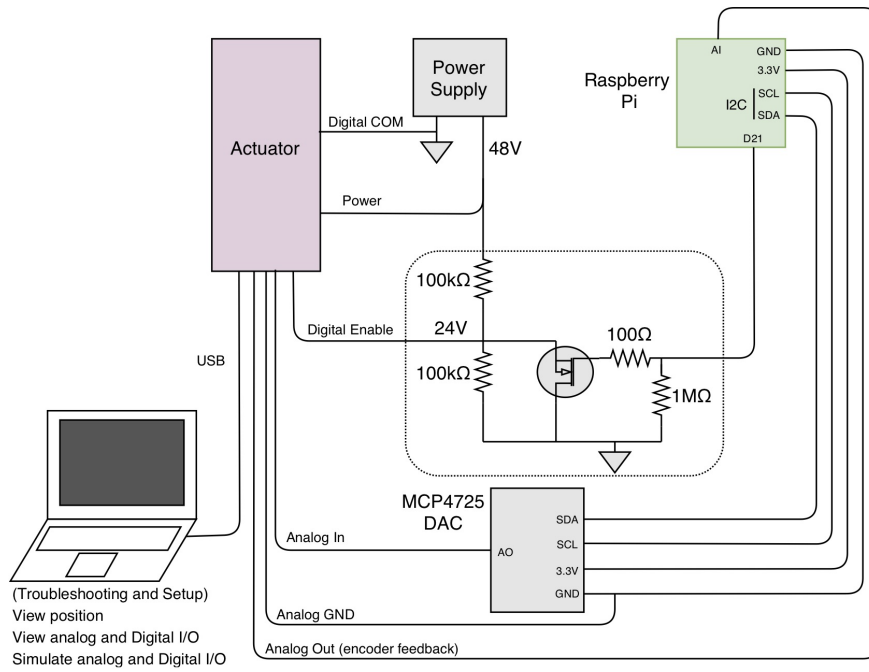


Figure 11: Schematic of analog position control setup.

443 via I2C to the DAC, where they are converted to analog voltages and input into the actuator,  
 444 thus generating the desired lung motion.

### 445 III. Results: Testing and Validation

446 To validate the efficacy of the piston and lung design, testing of the complete assembly was  
 447 performed. The primary criteria for evaluation were realism in the trajectory, symmetry  
 448 between the lungs, consistency of movement, and controllability.

449 The phantom was set up in the single O-ring configuration with the lungs not attached  
 450 to the piston, and was then filled with water. Filling was straightforward using the neck  
 451 ports. The lungs maintained their position and shape when opened to the atmosphere, and  
 452 the piston was then run back and forth continuously for 30 minutes with cameras mounted  
 453 above and on either side of the phantom. No water leakage to outside of the phantom  
 454 was observed. The piston was first set to move at 30mm/s and then 40mm/s, both with a  
 455 58mm amplitude. This corresponds to 892ml tidal volume at 15 and 21 breaths per minute,  
 456 respectively.

457 The resultant trajectory is shown in figure 12. The videos are available in the sup-  
 458 plementary materials. Qualitatively, the breathing looked realistic, and included some rib  
 459 motion and flexing, which adds to the realism. The lungs' maximum and minimum positions

---

### III. RESULTS: TESTING AND VALIDATION

460 were ascertained from the videos at all angles. There is little difference between the right  
 461 and left lung, as seen when viewed from above (figure 12, right image).

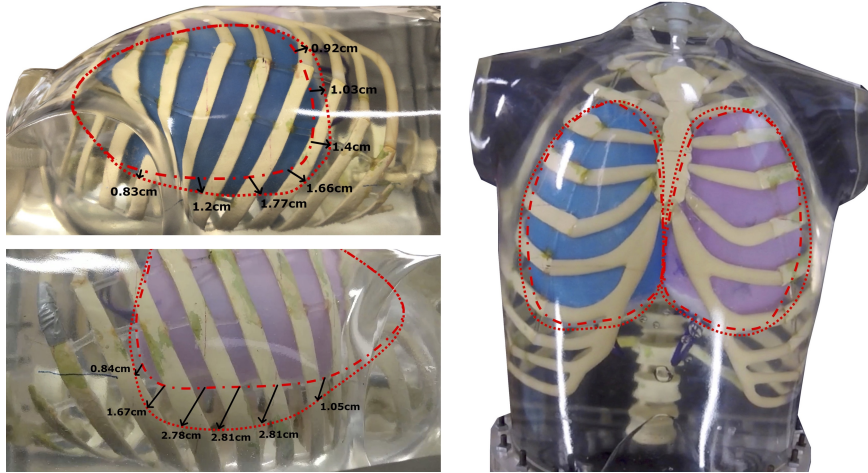


Figure 12: Screen grabs from the breathing test. The dotted lines indicate maximum inhalation, while the dashed lines are maximum exhalation. The tidal volume is 892ml. Note that the camera angle on the right and left lungs are slightly different to show a different cross-section of the trajectory. The view of both lungs show that they move almost identically.

462 Analysis of the actual displacements allows comparison to the average trajectories pre-  
 463 viously determined for adult males. The results are given in Table 3, in comparison with  
 464 previously published values<sup>7</sup>. These results show that the lungs naturally expand slightly  
 465 more in circumference and extend less axially than desired. However, they are within the  
 466 reasonable realistic adult male range given by Wade's measurements and his observation of  
 467 variability between individuals.

Table 3: Lung Trajectory Comparison. The 'scaled' column is the measured parameters normalized to match Wade's tidal volume for ease of comparison (assuming the parameters scale approximately linearly with volume in this range)

Parameter	Wade et al. <sup>7</sup>	Phantom	Scaled
Tidal Volume	$799 \pm 210\text{ml}$	892ml	799ml
Axial Extension	$1.7 \pm 0.26\text{cm}$	1.4cm	1.3
Circumference Increase	$6.8 \pm 2.2\text{cm}$	8.4cm	7.5cm

468 Finally, the consistency of the motion was analyzed by tracking three markers placed  
 469 on the left lung for 20 breaths using MATLAB. The frames were binned using the known  
 470 frame rate of the video and the set breathing rate such that only frames showing the lungs  
 471 at 100%, 75%, 50%, 25%, and 0% inhalation were used. The motion of each point formed  
 472 a scatter plot through which a line was fitted, and the root-mean-squared (RMS) error

473 was calculated as an indicator of the motion's consistency. The resulting RMS errors were  
474 0.74mm, 0.52mm, and 0.54mm from the straight line. Note that the tracking error in the  
475 position measurements was about  $\pm 1$ mm, so the results show that the lung motion was  
476 consistent between the breaths.

477 After a total of 40 minutes of almost continuous motion, the phantom was emptied,  
478 and the drive mechanism was dismantled and inspected. There were no signs of wear in the  
479 mechanism, which would have indicated a problem. The O-ring remained very well lubri-  
480 cated, and the cylinder wall behind the O-ring was dry. It is expected that with continued  
481 good lubrication and occasional O-ring replacement, the chance of leakage will remain very  
482 low. Since the phantom rests on an absorbent sheet throughout operation and is left in  
483 isolation until the isotopes have decayed to background levels, individual drops that may get  
484 through the piston do not represent a concern, especially as they remain contained within the  
485 cylinder. However, the second O-ring can also be installed on the piston to further improve  
486 the seal.

## 487 IV. Discussion

488 In normal respiration, lungs typically expand more axially than in cross-section<sup>7</sup>. In the  
489 developed phantom, the lung expansion was more uniform. Thus, artificial lesions attached  
490 to inferior lobes of the manufactured lungs will travel a shorter path on average compared  
491 to reality (for a similarly-sized person). Two approaches can be taken to increase the axial  
492 expansion. First, the lungs could be coupled directly to the piston using an elastic cord.  
493 Making this coupling looser or tighter would produce more or less axial extension, while  
494 also keeping the lungs centered in the antero-posterior direction. Alternatively, during the  
495 lung fabrication the wall material (Chlorosil) can be strategically rolled thinner in parts that  
496 should expand more.

497 In addition, though the ribs flex to accommodate the lung expansion, the torso shell  
498 is rigid, so the lungs are forced to expand dorsally instead of the chest rising as it does in  
499 humans. However, by attaching the lungs to the spine so they do not float up when the  
500 phantom is placed in a supine position, they can expand upwards during inhalation. In this  
501 way, lesions placed on the lungs near the chest retain the expected, anatomically correct  
502 trajectory.

503 A limitation of the phantom is that the lungs are filled with air, which makes it impos-

504 sible to place artificial lesions inside the lungs. Furthermore, the 511keV gamma attenuation  
505 coefficient is close to 0 inside the lungs, whereas in reality, it should be around 40% that of  
506 soft tissue<sup>17</sup>. We believe that both limitations can be addressed by filling the lungs with light  
507 and high-springback foam. If the foam is added inside the lungs in the compressed state, it  
508 can hold artificial lesions in place and expand with together with lungs, while also increasing  
509 the attenuation coefficient. The same method can be used to fill the space outside the lungs  
510 to introduce realistic image heterogeneity through small air bubbles caught in the foam and  
511 to facilitate organ placement, as shown previously in the Probe-IQ. Here the foam's effect on  
512 lung expansion, and the potential for all the bubbles to escape the foam under the constant  
513 motion must be assessed.

514 **V. Conclusion**

515 In this work we presented the mechanical design to incorporate realistic respiratory motion  
516 into the PROBE-IQ anthropomorphic phantom. The phantom can achieve a variety of  
517 respiratory wave-forms with up to 25 breaths per minute at 1232ml tidal volume. A new  
518 method to fabricate elastic lung models was established and tested. A software interface to  
519 plan and visualize these breathing patterns was developed, and two separate control schemes  
520 were proposed. The respiratory concept, mechanism, lungs, and control system were shown  
521 to be effective.

522 Some limitations were addressed in the discussion, and further tests are needed. Never-  
523 theless, the main aspects of the phantom design, including materials, fabrication, couplings,  
524 dynamics and usability have been validated. These elements can facilitate the construction  
525 of similar phantoms elsewhere, and guide the development of a next iteration of phantoms  
526 for PET/CT imaging. Once COVID-19 restrictions at our center are eased, CT scans will  
527 be performed at different phases of the respiratory cycles to more precisely characterize the  
528 motion. Pilot PET scans will also be performed to characterize the effect of lung motion on  
529 lesion quantification in a realistic environment. In future work, we will report the results of  
530 initial CT and PET scans, and investigate methods to further improve the realism of lung  
531 motion.

## 532 VI. Open Source

533 To promote further development of PET and phantom technology, we have open-  
534 sourced the entire design, including all CAD files, code, engineering drawings,  
535 and more, with supporting documentation. This material can be found here:  
536 <https://github.com/dgblack/robotPhantom>.

## 537 VII. Acknowledgements

538 We gratefully acknowledge support by Barber Prosthetics (Vancouver, Canada) in all as-  
539 pects related to lung manufacturing. The linear actuator for initial testing was provided by  
540 Robert de Rot at PQ Systems Ltd (Vancouver, Canada). We also gratefully acknowledge  
541 the Engineering Physics Project Lab at the University of British Columbia for financial and  
542 expertise support, as well as the BC Cancer Foundation for financial support.

## 543 References

- 545 1 P. E. Valk, E. Abella-Columna, M. K. Haseman, et al., Whole-body PET imaging with  
546 [18F]fluorodeoxyglucose in management of recurrent colorectal cancer., Arch. Surg. **134**,  
547 503–11; discussion 511–3 (1999).
- 548 2 S. A. Nehmeh, Y. E. Erdi, C. C. Ling, et al., Effect of respiratory gating on reducing  
549 lung motion artifacts in PET imaging of lung cancer, Med. Phys. **29**, 366 (2002).
- 550 3 L. Guerra, E. De Ponti, F. Elisei, et al., Respiratory gated PET/CT in a European  
551 multicentre retrospective study: added diagnostic value in detection and characterization  
552 of lung lesions, European Journal of Nuclear Medicine and Molecular Imaging **39**,  
553 1381–1390 (2012).
- 554 4 R. Manber, K. Thielemans, B. Hutton, et al., Clinical impact of respiratory motion  
555 correction in simultaneous PET/MR, using a joint PET/MR predictive motion model,  
556 Journal of Nuclear Medicine **59**, 1467–1493 (2019).
- 557 5 G. El Fakhri, Y. Rakvongthai, Magnetic resonance-based motion correction for quanti-  
558 tative PET in simultaneous PET-MR imaging, PET Clinics **12**, 321–327 (2017).
- 559 6 M. Dawood, N. Lang, X. Jiang, and K. P. Schäfers, Lung motion correction on respi-  
560 ratory gated 3-D PET/CT images., IEEE Trans. Med. Imaging **25**, 476–85 (2006).

- 561    7 O. Wade, Movements of the thoracic cage and diaphragm in respiration, Journal of  
562    Physiology **124**, 193–212 (1954).
- 563    8 F. Nayyeri, A review on motion correction methods in PET/CT images for detection of  
564    cancer cells, Acta Medica Bulgarica **42**, 68–78 (2015).
- 565    9 R. Schmitz, A. Alessio, and P. Kinahan, The physics of PET/CT scanners, Technical  
566    report, University of Washington.
- 567    10 A. Chi and N. Nguyen, 4D PET/CT as a strategy to reduce respiratory motion artifacts  
568    in FDG-PET/CT, Frontiers in Oncology **4**, 205 (2014).
- 569    11 S. S. Korreman, Motion in radiotherapy: photon therapy, Phys. Med. Biol. **57**, R161–  
570    R191 (2012).
- 571    12 X. Zhang, Z. Xie, E. Berg, et al., Total-Body Dynamic Reconstruction and Parametric  
572    Imaging on the uEXPLORER, J. Nucl. Med. **61**, 285–291 (2020).
- 573    13 R. J. Gillies, P. E. Kinahan, and H. Hricak, Radiomics: Images Are More than Pictures,  
574    They Are Data, Radiology **278**, 563–577 (2016).
- 575    14 K. Bolwin, B. Czekalla, L. Frohwein, F. Büther, and K. Schäfers, Anthropomorphic tho-  
576    rax phantom for cardio-respiratory motion simulation in tomographic imaging, Physics  
577    in Medicine and Biology **63** (2018).
- 578    15 I. Chrysanthou-Baustert, I. Polycarpou, O. Demetriadou, et al., Characterization of  
579    attenuation and respiratory motion artifacts and their influence on SPECT MP image  
580    evaluation using a dynamic phantom assembly with variable cardiac defects, Journal of  
581    Nuclear Cardiology **24**, 698–707 (2017).
- 582    16 D. Kadrmas, M. Casey, M. Conti, B. Jakoby, C. Lois, and D. Townsend, Impact of time-  
583    of-flight on PET tumor detection, Journal of Nuclear Medicine **50**, 1315–23 (2009).
- 584    17 D. Kadrmas, M. Casey, N. Black, J. Hamill, V. Panin, and M. Conti, Experimental  
585    comparison of lesion detectability for four fully-3D PET reconstruction schemes, IEEE  
586    Trans Med Imaging **28**, 523–34 (2009).

- 587 18 National Institute of Standards and Technology, X-Ray mass attenuation coefficients.  
588 <https://physics.nist.gov/PhysRefData/XrayMassCoef/tabc4.html>
- 589 19 Wikipedia, Lung volumes. [https://en.wikipedia.org/wiki/Lung\\_volumes](https://en.wikipedia.org/wiki/Lung_volumes)
- 590 20 D. Bhatt and K. Mistry, Experimental study of friction under different variables on a  
591 piston-cylinder assembly.
- 592 21 D. Merrit and F. Weinhaus, The pressure curve for a rubber balloon, American Journal  
593 of Physics **46**, 976–977 (1978).
- 594 22 K. Larson, Can you estimate modulus from durometer hardness for silicones?, 2019.
- 595 23 Tolomatic, ERD Electric Cylinder Features and Options. [www.tolomatic.com](http://www.tolomatic.com)
- 596 24 L. Cook, Rebreathing in the Mapleson A, C and D breathing systems with sinusoidal  
597 and exponential flow waveforms, Anaesthesia **52**, 1182–1194 (1997).